Published in final edited form as:
Exp Neurol. 2008 August ; 212(2): 448–457. doi:10.1016/j.expneurol.2008.04.033.

Magnetic resonance imaging of mouse skeletal muscle to measure denervation atrophy

Jiangyang Zhang[1*], **Gang Zhang**[2], **Brett Morrison**[2], **Susumu Mori**[1,3], and **Kazim A. Sheikh**[2*]

1*Department of Radiology, Johns Hopkins University School of Medicine, Baltimore, MD, USA*

2*Department of Neurology, Johns Hopkins University School of Medicine, Baltimore, MD, USA*

3*F.M. Kirby Functional Imaging Center, Kennedy Krieger Institute, Baltimore, MD, USA*

Abstract

We assessed the potential of different MRI measures to detect and quantify skeletal muscle changes with denervation in two mouse models of denervation/neurogenic atrophy. Acute complete denervation and chronic partial denervation were examined in calf muscles after sciatic nerve axotomy and in transgenic $SOD1^{G93A}$ mice, respectively. Serial T_2, diffusion tensor, and high resolution anatomical images were acquired, and compared to behavioral, histological, and electrophysiological data. Increase in muscle T_2 signal was first detected after sciatic nerve axotomy. Progressive muscle atrophy could be monitored with MRI-based volume measurements, which correlated strongly with postmortem muscle mass measurements. Significant increase in muscle fractional anisotropy and decreases in secondary and tertiary eigenvalues obtained from diffusion tensor imaging (DTI) were observed after denervation. In $SOD1^{G93A}$ animals, muscle denervation was detected by elevated muscle T_2 and atrophy in the medial gastrocnemius at 10 weeks. Changes in T_2 and muscle volume were first observed in medial gastrocnemius and later in other calf muscles. Alterations in secondary and tertiary eigenvalues obtained from DTI were first observed in tibialis anterior and medial gastrocnemius muscles at age 12 weeks. We propose that MRI of skeletal muscle is a sensitive surrogate outcome measure of denervation atrophy in animal models of neuromuscular disorders, with potential applicability in preclinical therapeutic screening studies in rodents.

Keywords

MRI; denervation; muscle atrophy; muscle size; nerve injury; SOD1

Neurogenic muscle atrophy is a common accompaniment of neuromuscular disorders affecting motor neurons, motor spinal roots, and peripheral nerves. Muscle size and/or function are frequently used to monitor neuromuscular diseases clinically as well as in disease models. Transgenic mice are often used as preclinical models of neuromuscular disorders. With the availability of various therapeutic interventions that are ready for preclinical evaluation of neuromuscular disorders, including motor neuron disease and neuropathies, there is increasing

*__Correspondence to: Jiangyang Zhang, Ph.D__, Address: Department of Radiology, Johns Hopkins University School of Medicine, 217 Traylor Bldg, 720 Rutland Ave., Baltimore, MD, 21205, USA, Email: jzhang3@jhmi.edu, __Kazim A. Sheikh, MD__, Address: Department of Neurology, Johns Hopkins University School of Medicine, 600 N-Wolfe street/509 Pathology Bldg., Baltimore, MD 21205, USA, Tel: 410-614-1196, Fax: 410-502-5459, Email: ksheik@jhmi.edu.

interest in sensitive biologic markers and outcome measures that not only detect the preclinical phase of these disorders, but can also monitor response to therapeutic interventions in the same animal without the need to sacrifice the animal. Development and availability of noninvasive diagnostic measures of muscle size and morphology would be a major advantage, particularly if these measures can follow the same animal over time and therefore are less sensitive to biologic variations among individuals. Such measures, once validated, could substitute for tedious morphologic and morphometric assays to assess muscle size and architecture, and achieve the desired statistical power in a preclinical drug trial with fewer animals. Overall, these features can reduce costs, effort, and importantly the time required for preclinical therapeutic screening studies.

Magnetic resonance imaging (MRI) is a useful technique for assessing muscle morphology and physiology. MRI of skeletal muscles has been used increasingly in clinical diagnosis of neuromuscular diseases, as well as in basic research on animal models. MRI can noninvasively examine muscle morphology and physiology with several quantitative measures, such as muscle volume (35), water and fat content (26), perfusion (25;34) and diffusion (10;36). Wessig et al. have reported that denervation in rat hindlimb muscles causes elevated longitudinal relaxation time (T_1) and transverse relaxation time (T_2), which return to baseline levels after reinnervation (37).

In the last decade, diffusion tensor imaging (DTI) has emerged as a novel technique to study tissue/muscle microstructure. DTI measures the extent of diffusion of water molecules in tissue along multiple directions and fits the results to a tensor model (2). DTI provides several indices that reflect tissue microstructures (e.g., diffusion anisotropy and mean diffusivity). The presence of highly ordered muscle fibers in the muscles makes DTI a useful tool to examine muscle structure/architecture. It has been shown that DTI can measure and reconstruct muscle fiber architecture in the heart, tongue, and calf muscles (11;15;21;29;33;36). Similarly, DTI has the potential to detect pathological conditions that affect the morphology of muscle and its organization. Recently, several groups have reported using DTI to study muscle injury and degeneration (19;20;38).

To assess the potential of different MRI measurements in detection and quantification of denervated muscles, we examined changes in muscle volume, T_2, and diffusion parameters in mouse models of denervation/neurogenic atrophy. Initially, MRI techniques were applied and validated after sciatic nerve axotomy, a model of complete muscle denervation. Because denervation is commonly partial and chronic in most neurogenic disorders, these studies were extended to a transgenic mouse line carrying a mutant form of human Cu^{+2}/ Zn^{+2} superoxide dismutase 1 ($SOD1^{G93A}$), found in some patients with amyotrophic lateral sclerosis (ALS), an animal model of chronic partial denervation.

Materials and Methods

Animals and Experimental Design

All experiments and procedures were approved by the Animal Care and Use Committee of the Johns Hopkins University, School of Medicine. A total of 46 mice were used in this study to examine complete and chronic partial denervation in two different animal models. *Complete denervation model*: Thirteen mice (C57BL/6J, male, 10~11 weeks, 4 controls, 6 with left sciatic nerve axotomy, and 3 with sham surgery) were used to correlate muscle mass and muscle fiber caliber with MRI measurements acquired at 25 days after left sciatic nerve axotomy. Mice with left sciatic nerve axotomy and controls (C57BL/6J, male, 10~11 weeks, n = 4 each) were used to study changes in muscle volume and T_2 after complete denervation. Sham operated animals were not included in this set of experiments because these animals were not different from untreated controls. T_2 map and high resolution anatomical images of the calf muscles were

acquired at 3 days before axotomy (baseline), at 3 days after axotomy, and weekly until 45 days after axotomy. *Chronic partial denervation model*: A line of $SOD1^{G93A}$ mutant mice designated as G1H or $SOD1^{G93A}$ expresses human $SOD1^{G93A}$ containing a substitution of $Gly^{93} \rightarrow Ala$. The current study examined this widely utilized high expressing $SOD1^{G93A}$ line (13-fold above endogenous $SOD1^{G93A}$) mutant (9;18), which is an extremely useful model for pathogenetic studies and preclinical drug screening and efficacy studies in ALS (7;17;27). Five each of $SOD1^{G93A}$ mice and age-matched littermate controls (n=10) were used to study the longitudinal changes in muscle T_2, muscle volume, and diffusion measurements in this animal model. T_2 map, high resolution anatomical images, and diffusion tensor images were acquired weekly, starting at age 9 weeks and continuing to 15 weeks. Longitudinal changes in muscle T_2, muscle volume, and diffusion measurements were reconfirmed in five additional $SOD1^{G93A}$ mice at age 15 and 16 weeks (n=5). The results obtained from these two separate studies are combined for presentation. Separate sets of animals (five each of $SOD1^{G93A}$ and control mice; n=10) were used for acquisition of behavior and electrophysiology. MRI data were correlated with behavioral and electrophysiological measures.

Sciatic Nerve Axotomy

Mice were deeply anesthetized with 1.5% isoflurane. Under sterile conditions, the left sciatic nerves were exposed at the level of the sciatic notch, tightly ligated with two sutures placed 5–6 mm apart and nerve was transected between these sutures. The sutures kept the proximal and distal stump from reconnection and prevented nerve regeneration in the distal stump. In sham control animals sciatic nerve was exposed but without nerve injury.

Electrophysiology

Electrophysiological measurements were done on the same $SOD1^{G93A}$ mice and age-matched littermate controls that underwent serial MRI exams at different time points. For technical and standardization issues, these measurements were restricted to lower limbs. CMAP amplitudes were recorded in the tibial innervated muscles (sole/flexor compartment) of the hind paws at weekly intervals with a PowerLab signal acquisition set up (AD Instruments). For these recordings, mice were anesthetized with 1.5% isoflurane, placed on heating pad at 37°C, and their body temperature was monitored with a rectal probe and maintained at 35°–37°C. The recording needle electrodes were inserted in the sole of the foot and the sciatic nerve was stimulated with needle electrodes at the sciatic notch, as described (24).

Behavior

The behavioral measurements were done on $SOD1^{G93A}$ and control mice. Behavioral evaluations included lower limb grip strength (13), which was measured weekly by means of a bar connected to an isometric force transducer (Grip strength meter, Columbus Instruments, Columbus OH). For this measurement, mice were lifted by their tails and made to hold a horizontal bar with their lower limbs/hind paws and then pulled backwards until they could no longer hold the grip. Maximal force (g) was registered during six consecutive attempts and averaged.

In vivo MRI

In vivo MRI was performed on an 11.7 Tesla NMR spectrometer (Bruker Biospin, Billerica, MA). During imaging, mice were anesthetized with 1% Isoflurane and a mixure of air and oxygen at 3:1 ratio by using a vaporizer. Body temperature was maintained at 35°–37 °C, and respiratory rate was monitored and maintained at 80–120 breaths/min by adjusting the anesthetic concentration. Images of mouse calves were acquired using a fast spin echo (FSE) sequence with twin navigator echoes for motion correction. T_2-weighted images at multiple echo times were acquired (TR/TE1/TE2/TE3 = 800/12/24/36 ms, ETL=4, fat suppression

enabled, 2 signal average and an imaging resolution of 0.15 mm × 0.15 mm × 0.5 mm). Muscle T_2 values were then calculated by Log-linear fitting. Coregistered high resolution anatomical imaging was acquired with a TR/TE = 800/18 ms, ETL=4, 2 signal average, and a resolution of 0.08 mm × 0.08 mm × 0.4 mm. The total imaging time for the T_2 measurements and high resolution anatomical imaging was approximately 1 hour. *In vivo* DTI data of mouse calf muscles were acquired using a 2D multiple slice multiple spin echo sequence with two echo acquisition, TR/TE of 2000/25 ms, two signal averages, an in-plane resolution of 0.17 mm × 0.2 mm, and a slice thickness of 1.5 mm. Images reconstructed from two echoes were added together to form one image to enhance signal to noise ratio (SNR). Seven diffusion-weighted images were acquired with δ = 5 ms / Δ = 10 ms. One image was acquired with a minimum *b* value (50 s/mm^2) and six images with maximum *b* value (500 s/mm^2). Diffusion sensitizing gradients were applied along six different orientations: [0.707, 0.707, 0], [0.707, 0, 0.707], [0, 0.707, 0.707], [−0.707, 0.707, 0], [0.707, 0, −0.707], [0, −0.707, 0.707]. The imaging time for DTI was approximately 40 minutes. The SNR of the images with minimum b value were approximately 25. The diffusion-weighted images were transferred to an offline workstation and processed using DtiStudio (S. Mori and H. Jiang, Johns Hopkins University, http://lbam.med.jhmi.edu). The six elements of diffusion tensor were determined by Log-linear fitting. The tensor was diagonalized to obtain the primary, secondary, and tertiary eigenvalues (λ_1, λ_2, λ_3, respectively), where λ_1 is the largest eigenvalue and λ_3 is the smallest eigenvalue. Fractional anisotropy (FA) (4) was calculated as follows:

$$FA = \frac{\sqrt{((\lambda_1 - \lambda_2)^2 + (\lambda_2 - \lambda_3)^2 + (\lambda_1 - \lambda_3)^2)}}{\sqrt{2(\lambda_1^2 + \lambda_2^2 + \lambda_3^2)}}$$

Image processing

Anatomical and T_2 Images were separated into left and right legs, respectively, and were individually normalized to a selected template (images from selected animals). The normalization was performed using rigid transformation based on 9 landmarks defined at the joints and bones. This normalization procedure is necessary for examination of muscle atrophy, either by visual inspection or quantitative comparison of muscle cross-sectional areas at arbitrary axial planes between the knee and ankle joints. Manual segmentation of the bones and five muscles (tibialis anterior, soleus, medial and lateral gastrocnemius, and plantaris) was performed using Amira 3.1 (Mercury Computer System Inc., San Diego, CA) on the normalized images. The boundaries of individual muscles in axial images were manually traced as defined in Greene's Rat Anatomy Atlas and a recently published mouse atlas (16;22). Examples of our 2D segmentation and 3D rendering of segmented bones and muscles are shown in Figure 1. From the segmentation results, volumes of the five muscles were obtained.

Histological analysis of muscle

Denervated and contralateral nondenervated gastrocnemius and tibialis anterior muscles were harvested and weighed. These muscles were frozen in dry ice-cooled isopentane and 10-μm cross-sections of muscle were obtained from the middle of the gastrocnemius and stained with hematoxylin and eosin. Muscle fiber diameters were quantified using Openlab software on a Mac PowerPC G4 computer attached to a Zeiss Axiophot microscope. Fiber diameter was defined as "the greatest distance between the opposite sides of the narrowest aspect of the fiber" (6). Three-hundred consecutive muscle fibers per animal were quantified from both the denervated and contralateral non-denervated muscles.

Statistical Analysis

Group comparisons on muscle volumes and weight and mean muscle fiber diameter were performed using Student's *t*-test (IDL, Research System Inc., Boulder, CO, USA), threshold

for statistical significance set at $p = 0.05$. For the complete denervation model, the percent reduction in muscle volume after denervation was calculated by dividing individual muscle volume with respect to its baseline volume. Group comparisons on the percent reduction in muscle volume at each time point were performed using two-way analysis of variance (ANOVA) with the threshold for statistical significance set at $p = 0.05$. The two null hypotheses were: (1) nerve injury does not affect muscle volumes; and (2) tibialis anterior, medial gastrocnemius, and lateral gastrocnemius muscles do not differ in the percent reduction in muscle volume. T_2 and diffusion measurements on wild type animals with sciatic nerve axotomy and $SOD1^{G93A}$ and littermate control animals, were analyzed by nonparametric rank sum test, threshold for statistical significance set at $p = 0.05$. Correlations between MRI volume measurements and muscle weights and between muscle weights and average muscle fiber diameters were done with linear regression analysis (SigmaPlot; Systat Inc., San Jose, CA, USA), significance threshold set at $p = 0.01$.

Results

Validation studies

Initial validation studies were done at 25 days after the nerve axotomy because at that time the muscle atrophy could be discerned visually. MR images of denervated and contralateral calf muscles showed significant reduction in muscle cross-sectional area (Fig. 2A and C). Three-dimensional reconstructions of major muscles, based on manual segmentation (Fig. 2B and D), permitted visualization of the atrophy of denervated muscles with respect to the contralateral intact muscles. Histology of the tibialis anterior and gastrocnemius (Fig. 2E–H) revealed atrophy in muscle fibers and enlarged extracellular spaces, with significant decrease in muscle weight and mean muscle fiber diameter in denervated muscles ($p < 0.01$, Fig. 2I–J). The percent reduction in terms of MRI muscle volume and muscle weight and muscle fiber diameter was more severe in the gastrocnemius than in the tibalis anterior muscle (Fig. 2I–K). There were strong correlations between muscle weight and mean muscle fiber diameter (Fig. 2L) and between muscle weight and muscle volumes obtained by MRI (Fig. 2M). The muscle volume, weight, and muscle fiber diameter in sham operated animals did not differ from untreated controls.

Complete denervation model

Longitudinal MRI studies showed progressive loss of muscle volume in the sciatic nerve axotomy model (Fig. 3). Compared to the baseline, reduction in muscle cross-sectional area in denervated muscles first became apparent at 10 days after axotomy, and continued to progress. Muscles on the contralateral side or uninjured control animals showed no significant change in the volume over the course of these MRI studies. Volume measurements (Fig. 3) showed that the degree and rate of atrophy were not uniform among the segmented muscles, even though all the muscles are innervated by the transected sciatic nerve or its branches. Denervation induced relatively more severe atrophy in the gastrocnemius muscle than in the tibialis anterior muscle. During the first 2 weeks, atrophy progressed at a higher rate in the gastrocnemius than in the tibialis anterior muscle. Two weeks after axotomy, the total volumes of the medial and lateral gastrocnemius muscles were reduced to approximately 50% of their baseline values (37% ± 2.0% for the medial gastrocnemius muscle and 54% ± 5.2% for the lateral gastrocnemius muscle), while the tibialis anterior muscle remained approximately 76% (± 9%) of its baseline value. The atrophy in tibialis anterior at 14 days was significantly less than in gastrocnemius muscles (two-way ANOVA, $p = 0.04$). At 45 days after axotomy, the gastrocnemius muscles showed the most severe atrophy (19% ± 7.2% for the medial and 38% ± 6.4% for the lateral gastrocnemius muscles compared to baseline). In contrast, the tibialis anterior muscle maintained approximately 57% ± 3.8% of its average baseline volume. The atrophy in tibialis anterior at 45 days was significantly less than in gastrocnemius muscles

(two-way ANOVA, $p = 0.004$). The relative atrophy of the soleus and the plantaris muscles was in the intermediate range compared to tibialis anterior and gastrocnemius muscles (Fig. 3 E–F).

Elevation in muscle T_2 value in denervated muscles had been reported in previous studies (5; 14) and was detected in our study at 3 days after axotomy, and remained elevated during the entire study period (Fig. 4). Increase in T_2 values in denervated muscles compared to corresponding muscles on the uninjured side was approximately 2 ~ 4 ms, which although small, could be appreciated qualitatively from T_2 map images. T_2 increase was most marked between 3–10 days after axotomy and this increase in T_2 signal declined after this time period but remained significantly elevated compared to baseline. No significant differences in the amount of T_2 increase were detected among different muscles.

Diffusion tensor measurements of calf muscles at 25 days after sciatic nerve axotomy (Fig. 5) showed that the fractional anisotropy (FA) values in denervated muscles were significantly higher than the FA values in muscles on the uninjured side, sham, and uninjured control mice, although the difference was small (~ 0.1). The secondary (λ_2) and tertiary (λ_3) eigenvalues, which measure the extent of water diffusion perpendicular to the direction of muscle fibers, were significantly lower in the denervated muscles than in the muscles on the uninjured side, sham, and uninjured control mice (Fig. 5). No significant change in primary eigenvalue (λ_1), which measures the extent of water diffusion along the direction of the muscle fibers, was detected (Fig. 5).

Chronic denervation model

Temporal changes in muscle volume, T_2, and diffusion measurements in 10- to 15- week-old $SOD1^{G93A}$ animals are shown in Fig. 6 and Table 1. MR-based volume measurements (Fig. 6 A,B) showed progressive muscle atrophy and detected significant atrophy at age 10 weeks in the medial gastrocnemius and at 11 weeks in the tibialis anterior compared to measurements obtained in age-matched controls. We believe that these changes are due to denervation atrophy, because the T_2 signal also increased at this time point and previous morphological studies document denervation at this age (9;13). When volume of the entire calf muscles was used to detect atrophy, significant decrease was observed at age 13 weeks (Table 1). The medial gastrocnemius showed rapid atrophy and its volume was reduced to approximately 60% of the volumes in control mice at 11 weeks of age, while the volumes of the tibialis anterior and whole calf remained above 70% of control values until 14 weeks of age. At 15–16 weeks, both medial gastrocnemius and tibialis anterior showed significant atrophy. Notably, muscle T_2 values (Fig. 6C) showed significant increases at age 10 weeks in the medial gastrocnemius and at age 11 weeks in the tibialis anterior muscles. FA measurements (Fig. 6D) showed no significant changes over the study period. The secondary and tertiary eigenvalues (λ_2 and λ_3, respectively) showed significant decrease in both MG and TA in 12-week-old mice. No significant changes in the primary eigenvalue (λ_1) was detected at any age (data not shown). Hind paw muscle CMAP amplitudes and grip strength showed progressive decline over the study period in $SOD1^{G93A}$ animals (Table 2), as reported previously (1;12).

Discussion

Our study shows that different MRI parameters are extremely useful and sensitive markers for detection and measurement of acute and chronic muscle atrophy due to denervation in living mice. Three different MRI measures were applied to two different mouse models to evaluate the applicability of these parameters to monitor denervation atrophy. The MRI parameters examined in this study are not specific for denervation atrophy but can overlap with conditions affecting muscles primarily (19;20;38). Nonetheless, this does not diminish the utility of this technique because the pathogenic basis (neurogenic versus myopathic) of muscle atrophy is

usually well defined in neuromuscular models generated experimentally. Because MRI is a noninvasive measure that can be serially applied to the same animal, our studies support the use of MRI as an outcome measure in preclinical studies in rodent models of neuromuscular disorders.

In the current study we compared an acute and complete denervation sciatic nerve axotomy model to a chronic model of partial denervation resulting from motor neuron degeneration. The sciatic nerve axotomy model provides uniform denervation in all studied muscles and is better suited for correlating MR measurements and muscle denervation without the confounding effect of reinnervation, whereas muscles of $SOD1^{G93A}$ mice have ongoing chronic denervation and reinnervation. These models were selected because acute and complete denervation is typical of nerve transection that is sometimes seen in traumatic nerve injuries, whereas most neurogenic disorders, including motor neuron disorders and axonal polyneuropathies, induce partial and chronic denervation and reinnervation.

Currently, the outcome measures of muscle denervation in rodents include behavioral, electrophysiological, and histological parameters. Histological and electrophysiological examination measures the integrity of motor units and serves as a surrogate marker for motor neuron number and motor nerve fiber integrity. The behavioral tests such as grip strength are easy to perform serially and their abnormalities define the onset of clinical weakness, but this kind of behavioral testing does not detect the preclinical phase of neuromuscular changes that have been documented by pathological studies, for example in $SOD1^{G93A}$ mice. Currently used quantitative strength measurements are almost exclusively restricted to limb or appendicular musculature in the hind limbs and do not assess axial/truncal musculature. Further, these measurements provide only low sensitivity for detecting changes in the muscle strength, particularly during the progressive and end stages of disease (12). Moreover, behavioral tests are complicated because they can be affected by complex variables including psychoenvironmental factors. Similarly, electrophysiological measures such as compound motor action potential (CMAP) amplitudes or motor unit number estimation (MUNE) have been used mostly for the distal hind limb musculature (23;31;32) and their widespread application is precluded by standardization issues, operator dependency, and reproducibility (1;23;30;32). Histology is most commonly used as an outcome measure in most preclinical therapeutic trials. Although the morphological and morphometric analysis of motor neurons, peripheral nerves, or muscles is currently considered the gold standard for denervation, the limitations of these measures include the need to kill the animal, so that the technique cannot be used serially on the same animal, and it requires laborious and cumbersome morphometric techniques.

T_2 relaxation time was the earliest change detected by MRI in both acute and chronic denervation models. Increase in T_2 preceded muscle atrophy by several days in the acute axotomy model. In $SOD1^{G93A}$ mice the increase in T_2 signal correlated with the onset of muscle atrophy in individual muscles at age 10 weeks. The possibility of increase in T_2 signal preceding atrophy in $SOD1^{G93A}$ mice is not excluded, because earlier time points were not examined. Currently, the mechanism(s) that result in T_2 increase in denervated muscles are still unknown. A previous study has suggested that hyperperfusion due to denervation of arterioles in muscles may cause the increase in T_2 (37), which could also occur in the acute nerve axotomy model examined in this study. The mechanisms involved in T_2 change are likely to be more complicated, however, because increase in T_2 was also seen in $SOD1^{G93A}$ mice in which relatively selective degeneration of motor neurons is the predominant pathology. The difference in muscle T_2 between normal and denervated muscles measured on our 11.7 Tesla MR scanner (~ 3 ms) was smaller than the values reported previously in rats obtained on a 1.5 Tesla MR scanner (~13 ms) (37). Tissue T_2 values shorten when moving from low magnetic

field (1.5 Tesla) to high magnetic field (11.7 Tesla in this study), thus providing one explanation for the differences in T_2 changes observed in the two studies.

Although muscle T_2 is sensitive to the onset of denervation, it is not an ideal measure for quantifying progression of muscle atrophy. As shown in Fig. 3 and a previous report (37), muscle T_2 stayed relatively unchanged, while denervated muscles underwent progressive atrophy. In contrast, anatomical 3D MRI measuring volume can provide dynamic information about denervation atrophy over time. In the sciatic nerve axotomy model, we found that the extent and progression of muscle atrophy varied among different calf muscles. For example, the medial and lateral gastrocnemius muscles showed decreases in muscle volume before the tibialis anterior muscle. Further, the rate of atrophy was more rapid and extent of muscle atrophy was more advanced in gastrocnemius muscles compared to the tibialis anterior muscle. This finding was also reconfirmed by muscle mass measurements (see Fig. 2). Similar findings were observed in $SOD1^{G93A}$ mice: medial gastrocnemius muscle (significant change ~10 weeks) atrophy preceded that of tibialis anterior (significant change ~11 weeks) and entire calf (significant change ~13 weeks) muscle volume. The basis of differential muscle atrophy in the posterior and anterior compartment muscles is not clear. Both muscles are primarily fast muscles, with 87% of fibers from medial gastrocnemius and 100% of fibers from tibialis anterior being fast-twitch glycolytic or fast-twitch oxidative glycolytic (8). Interestingly, decreased atrophy of tibialis anterior compared to medial gastrocnemius muscle was also observed following spinal cord isolation in a previous study (28) and the authors suggested that this was related to higher basal activity (as measured by 24-hour EMG) of medial gastrocnemius compared to tibialis anterior. When this activity was reduced to zero, greater loss of activity in medial gastrocnemius compared to tibialis anterior led to greater atrophy.

We observed decreases in the secondary and tertiary eigenvalues in the complete denervation and chronic denervation models. A possible basis of this change is the reduced muscle fiber diameter and enlarged extracellular space. Previous studies propose that DTI measurements of skeletal muscles mainly reflect the properties of intracellular water diffusion (11;15). In a recent study of ischemia, increase in mean diffusivity and the smallest eigenvalues were correlated with swollen myocytes (20). Our findings are in line with these previous observations, and suggest that the second and tertiary eigenvalues are markers of myofiber atrophy. The advantage of DTI measurements in detecting muscle atrophy compared to volume measurements is that DTI measurements do not require time-consuming segmentation of individual muscles. There is a concern that at SNR values <10 significant bias in the estimation of the eigenvalues and FA caused by background noise can occur so that increase in background noise will cause artificially increased FA and λ_1 and decreased λ_3 (3). This concern is not applicable to our findings because SNR in our studies was ~ 25.

Our studies demonstrate the feasibility of measuring T_2 signal and DTI measurements at the level of individual muscles and 3D reconstructions and measurement of individual muscle volume. We detected T_2 signal changes and muscle atrophy in $SOD1^{G93A}$ mice at age 10 weeks before the onset of clinical signs in hindlimbs of these animals, which start at ~90 days of age (18). These techniques are relatively sensitive for detecting and monitoring the denervation atrophy in both acute and chronic models. 3D imaging examining the entire calf muscle is superior to the conventional approach of measuring the circumference or cross-sectional area of muscles with high resolution MRI or CT. This is particularly true for longitudinal studies; it is often difficult to ensure consistent measurement of the exact same area/slice in serial scans because muscle tissue is malleable and has a tendency to deform with external force/pressure.

In summary, we show that MRI of skeletal muscle is a sensitive surrogate measure of motor unit integrity in limb musculature that can be extended to axial or truncal muscles. Such a technique has the potential to substitute for tedious morphologic and morphometric assays to

quantify motor neuron or peripheral nerve injury. We have already shown the feasibility of muscle MRI as an outcome measure in a peripheral nerve injury and regeneration model (24). Since *in vivo* MRI can be serially applied to the same animal, this technique can achieve the desired statistical power in a preclinical drug trial with fewer animals. The MR data can be processed and analyzed immediately after acquisition. Overall, these features reduce costs, effort, and importantly the time required for preclinical therapeutic screening studies.

Acknowledgements

This work was supported by grants from Muscular Dystrophy Association (MDA4037), Dr. Miriam and Sheldon G. Adelson Medical Research Foundation, and the National Institute of Health (NS42888, NS54962, and NS37096). We thank Drs. John Griffin, Bruce Dobkin, John Mazziotta, and Ahmet Hoke for helpful suggestions and advice and Dr. Pamela Talalay for editorial discussion.

References

1. Azzouz M, Leclerc N, Gurney M, Warter JM, Poindron P, Borg J. Progressive motor neuron impairment in an animal model of familial amyotrophic lateral sclerosis. Muscle Nerve 1997;20:45–51. [PubMed: 8995582]
2. Basser PJ, Mattiello J, Lebihan D. Mr Diffusion Tensor Spectroscopy and Imaging. Biophysical Journal 1994;66:259–267. [PubMed: 8130344]
3. Basser PJ, Pajevic S. Statistical artifacts in diffusion tensor MRI (DT-MRI) caused by background noise. Magnetic Resonance in Medicine 2000;44:41–50. [PubMed: 10893520]
4. Basser PJ, Pierpaoli C. Microstructural and physiological features of tissues elucidated by quantitative-diffusion-tensor MRI. Journal of Magnetic Resonance Series B 1996;111:209–219. [PubMed: 8661285]
5. Bendszus M, Koltzenburg M, Wessig C, Solymosi L. Sequential MR imaging of denervated muscle: experimental study. AJNR Am.J.Neuroradiol 2002;23:1427–1431. [PubMed: 12223392]
6. Brooke MH, Engel WK. Histographic Analysis of Human Muscle Biopsies with Regard to Fiber Types . 4. Childrens Biopsies. Neurology 1969;19:591-&. [PubMed: 5814304]
7. Bruijn LI, Cleveland DW. Mechanisms of selective motor neuron death in ALS: insights from transgenic mouse models of motor neuron disease. Neuropathol.Appl.Neurobiol 1996;22:373–387. [PubMed: 8930947]
8. Burkholder TJ, Fingado B, Baron S, Lieber RL. Relationship Between Muscle-Fiber Types and Sizes and Muscle Architectural Properties in the Mouse Hindlimb. Journal of Morphology 1994;221:177–190. [PubMed: 7932768]
9. Chiu AY, Zhai P, Dal Canto MC, Peters TM, Kwon YW, Prattis SM, Gurney ME. Age-dependent penetrance of disease in a transgenic mouse model of familial amyotrophic lateral sclerosis. Mol.Cell Neurosci 1995;6:349–362. [PubMed: 8846004]
10. Cleveland GG, Chang DC, Hazlewood CF, Rorschach HE. Nuclear Magnetic-Resonance Measurement of Skeletal-Muscle - Anisotropy of Diffusion-Coefficient of Intracellular Water. Biophysical Journal 1976;16:1043–1053. [PubMed: 963204]
11. Damon BM, Ding ZH, Anderson AW, Freyer AS, Gore JC. Validation of diffusion tensor MRI-based muscle fiber tracking. Magnetic Resonance in Medicine 2002;48:97–104. [PubMed: 12111936]
12. Derave W, Van Den BL, Lemmens G, Eijnde BO, Robberecht W, Hespel P. Skeletal muscle properties in a transgenic mouse model for amyotrophic lateral sclerosis: effects of creatine treatment. Neurobiol.Dis 2003;13:264–272. [PubMed: 12901841]
13. Fischer LR, Culver DG, Tennant P, Davis AA, Wang M, Castellano-Sanchez A, Khan J, Polak MA, Glass JD. Amyotrophic lateral sclerosis is a distal axonopathy: evidence in mice and man. Exp.Neurol 2004;185:232–240. [PubMed: 14736504]
14. Fleckenstein JL, Watumull D, Conner KE, Ezaki M, Greenlee RG, Bryan WW, Chason DP, Parkey RW, Peshock RM, Purdy PD. Denervated Human Skeletal-Muscle - Mr Imaging Evaluation. Radiology 1993;187:213–218. [PubMed: 8451416]

15. Galban CJ, Maderwald S, Uffmann K, de Greiff A, Ladd ME. Diffusive sensitivity to muscle architecture: a magnetic resonance diffusion tensor imaging study of the human calf. European Journal of Applied Physiology 2004;93:253–262. [PubMed: 15322853]
16. Greene, EC. The anatomy of the Rat. New York: Hafner Publishing; 1963.
17. Gurney ME. The use of transgenic mouse models of amyotrophic lateral sclerosis in preclinical drug studies. J.Neurol Sci 1997;152:S67–S73. [PubMed: 9419057]
18. Gurney ME, Pu H, Chiu AY, Dal Canto MC, Polchow CY, Alexander DD, Caliendo J, Hentati A, Kwon YW, Deng HX, et al. Motor neuron degeneration in mice that express a human Cu,Zn superoxide dismutase mutation. Science 1994;264:1772–1775. [PubMed: 8209258]
19. Heemskerk AM, Drost MR, van Bochove GS, van Oosterhout MFM, Nicolay K, Strijkers GJ. DTI-based assessment of ischemia-reperfusion in mouse skeletal muscle. Magnetic Resonance in Medicine 2006;56:272–281. [PubMed: 16826605]
20. Heemskerk AM, Strijkers GJ, Drost MR, van Bochove GS, Nicolay K. Skeletal muscle degeneration and regeneration after femoral artery ligation in mice: Monitoring with diffusion MR imaging. Radiology 2007;243:413–421. [PubMed: 17384238]
21. Heemskerk AM, Strijkers GJ, Vilanova A, Drost MR, Nicolay K. Determination of mouse skeletal muscle architecture using three-dimensional diffusion tensor imaging. Magnetic Resonance in Medicine 2005;53:1333–1340. [PubMed: 15906281]
22. Iwaki, T.; Yamashita, H.; Hayakawa, T. A Color Atlas of Sectional Anatomy of the Mouse. Tokyo: Adthree Pub. Co; 2001.
23. Kennel PF, Finiels F, Revah F, Mallet J. Neuromuscular function impairment is not caused by motor neurone loss in FALS mice: an electromyographic study. Neuroreport 1996;7:1427–1431. [PubMed: 8856691]
24. Lehmann HC, Lopez PHH, Zhang G, Ngyuen T, Zhang JY, Kieseier BC, Mori S, Sheikh KA. Passive immunization with anti-ganglioside antibodies directly inhibits axon regeneration in an animal model. J.Neurosci 2007;27:27–34. [PubMed: 17202469]
25. Luo YP, Mohning KM, Hradil VP, Wessale JL, Segreti JA, Nuss ME, Wegner CD, Burke SE, Cox BF. Evaluation of tissue perfusion in a rat model of hind-limb muscle ischemia using dynamic contrast-enhanced magnetic resonance imaging. Journal of Magnetic Resonance Imaging 2002;16:277–283. [PubMed: 12205583]
26. Phoenix J, Betal D, Roberts N, Helliwell TR, Edwards RHT. Objective quantification of muscle and fat in human dystrophic muscle by magnetic resonance image analysis. Muscle Nerve 1996;19:302–310. [PubMed: 8606693]
27. Rothstein JD. Of mice and men: reconciling preclinical ALS mouse studies and human clinical trials. Ann Neurol 2003;53:423–426. [PubMed: 12666108]
28. Roy RR, Zhong H, Siengthai B, Edgerton VR. Activity-dependent influences are greater for fibers in rat medial gastrocnemius than tibialis anterior muscle. Muscle Nerve 2005;32:473–482. [PubMed: 15962333]
29. Scollan DF, Holmes A, Winslow R, Forder J. Histological validation of myocardial microstructure obtained from diffusion tensor magnetic resonance imaging. American Journal of Physiology-Heart and Circulatory Physiology 1998;44:H2308–H2318.
30. Shefner JM, Brown RH Jr, Cole D, Chaturvedi P, Schoenfeld D, Pastuszak K, Matthews R, Upton-Rice M, Cudkowicz ME. Effect of neurophilin ligands on motor units in mice with SOD1 ALS mutations. Neurology 2001;57:1857–1861. [PubMed: 11723276]
31. Shefner JM, Cudkowicz ME, Brown RH Jr. Comparison of incremental with multipoint MUNE methods in transgenic ALS mice. Muscle Nerve 2002;25:39–42. [PubMed: 11754183]
32. Shefner JM, Reaume AG, Flood DG, Scott RW, Kowall NW, Ferrante RJ, Siwek DF, Upton-Rice M, Brown RH Jr. Mice lacking cytosolic copper/zinc superoxide dismutase display a distinctive motor axonopathy. Neurology 1999;53:1239–1246. [PubMed: 10522879]
33. Sinha S, Sinha U, Edgerton VR. In vivo diffusion tensor imaging of the human calf muscle. Journal of Magnetic Resonance Imaging 2006;24:182–190. [PubMed: 16729262]
34. Streif JUG, Hiller KH, Waller C, Nahrendorf M, Wiesmann F, Bauer WR, Rommel E, Haase A. In vivo assessment of absolute perfusion in the murine skeletal muscle with spin labeling MRI. Journal of Magnetic Resonance Imaging 2003;17:147–152. [PubMed: 12500285]

35. Tracy BL, Ivey FM, Metter EJ, Fleg JL, Siegel EL, Hurley BF. A more efficient magnetic resonance imaging-based strategy for measuring quadriceps muscle volume. Medicine and Science in Sports and Exercise 2003;35:425–433. [PubMed: 12618571]

36. Wedeen VJ, Reese TG, Napadow VJ, Gilbert RJ. Demonstration of primary and secondary muscle fiber architecture of the bovine tongue by diffusion tensor magnetic resonance imaging. Biophysical Journal 2001;80:1024–1028. [PubMed: 11159469]

37. Wessig C, Koltzenburg M, Reiners K, Solymosi L, Bendszus M. Muscle magnetic resonance imaging of denervation and reinnervation: correlation with electrophysiology and histology. Exp.Neurol 2004;185:254–261. [PubMed: 14736506]

38. Zaraiskaya T, Kumbhare D, Noseworthy MD. Diffusion tensor imaging in evaluation of human skeletal muscle injury. Journal of Magnetic Resonance Imaging 2006;24:402–408. [PubMed: 16823776]

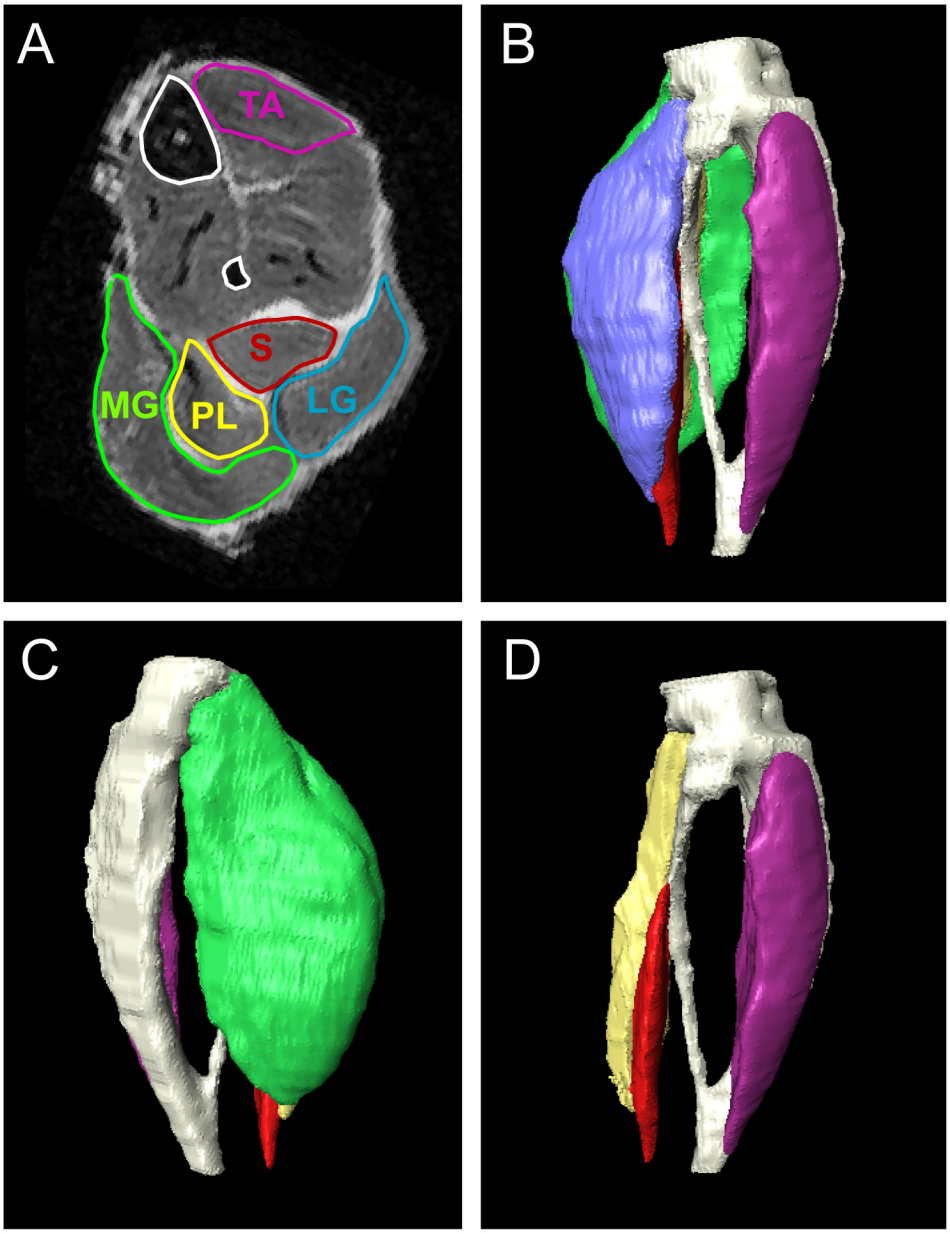

Figure 1.
Manual segmentation of high resolution MR images of mouse calf muscles (A). 3D reconstructions of calf muscles are shown (B–D), with bones rendered as white structures. (B) lateral and (C) medial views of 3D reconstruction of all calf muscles. (D) lateral view of 3D reconstruction of calf muscles after removal of medial and lateral gastrocnemius muscles. Abbreviations: LG = lateral gastrocnemius; MG = medial gastrocnemius; PL = plantaris; S = soleus; TA = tibialis anterior.

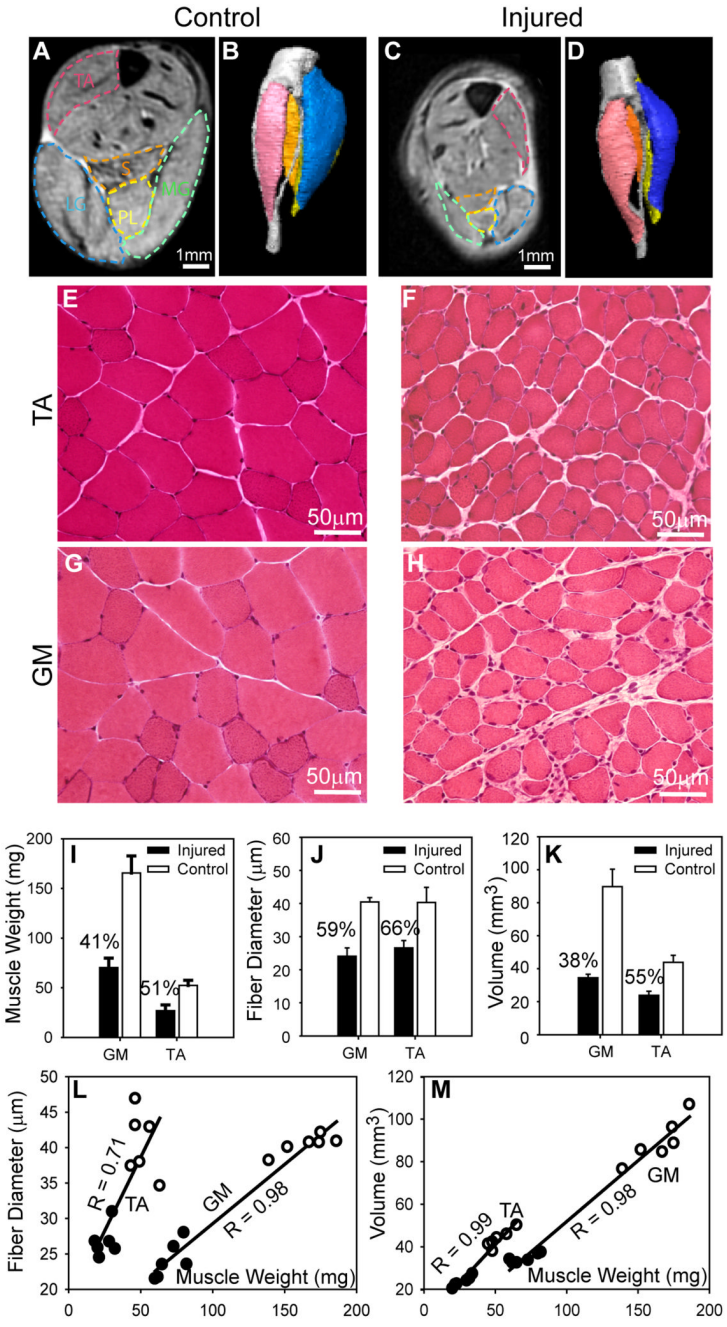

Figure 2.

Correlation of anatomical MRI with morphology. A–D: Axial anatomical MR images (A&C) and 3D reconstructions (B&D) of the tibialis anterior (TA), soleus (S), plantaris (PL), medial and lateral gastrocnemius (MG and LG, respectively) muscles on the denervated (injured) and contralateral (control/uninjured) sides at 25 days after sciatic nerve axotomy showing denervation atrophy. Manually defined muscle boundaries are overlaid on MR images. E–H: Fresh frozen sections of the TA and gastrocnemius (GM) on the uninjured side (left panels) and contralateral injured side (right panels). I&J: Percentage change in muscle weights (I), fiber diameters (J), and MRI muscle volumes (K) in TA and GM on the denervated side (black bars) compared to uninjured contralateral side (white bars) showing atrophy of denervated

muscles (I,K) and muscle fibers (J). L: Correlation between muscle mass and muscle fiber diameters in denervated (black circles) and uninjured (white circles) muscles. M: Correlation between muscle mass and muscle volume (measured by MRI) in denervated (black circles) and uninjured (white circles) muscles.

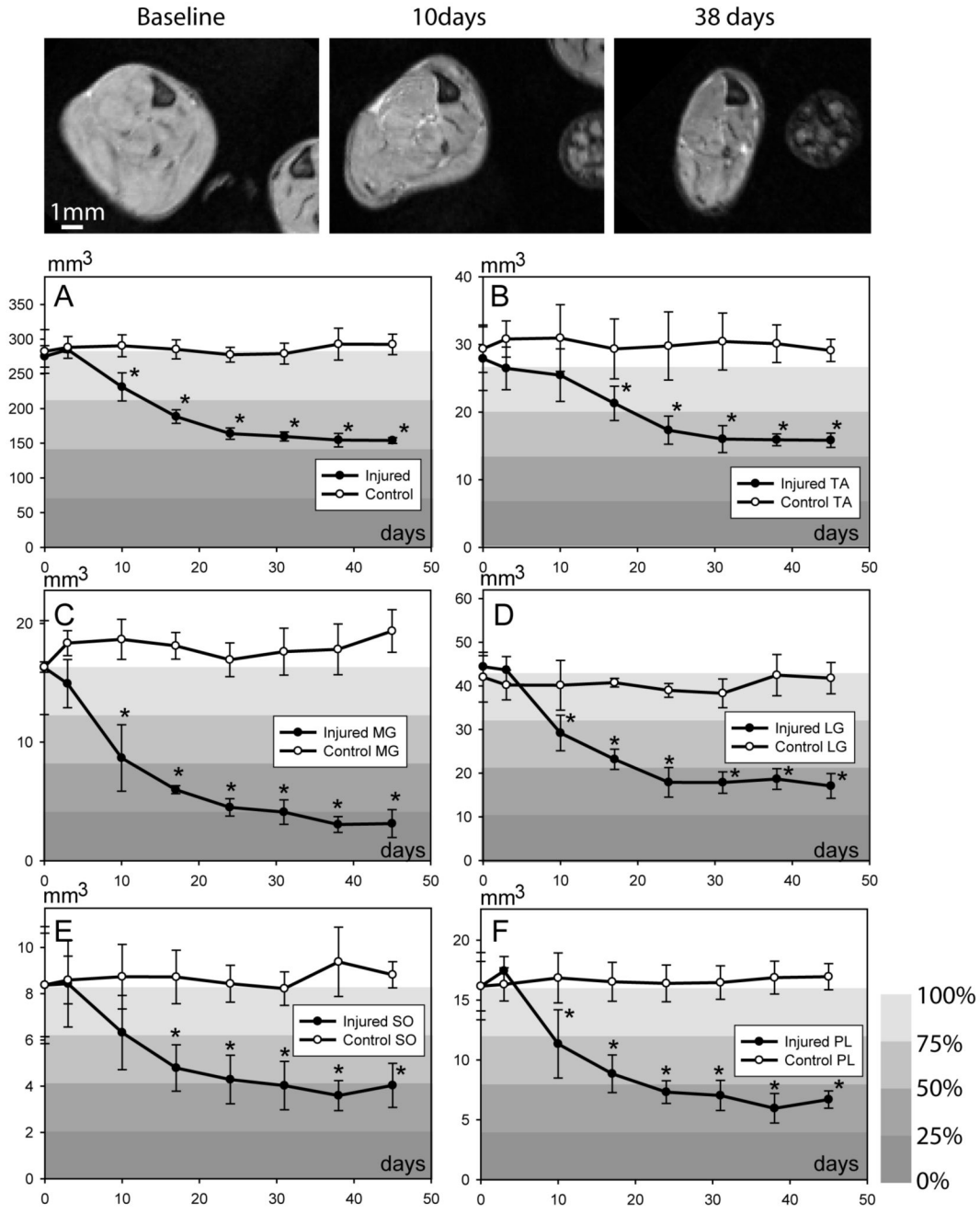

Figure 3.

Temporal changes in the calf muscle volumes before and after complete denervation shown in axial images (top panel). A–F: Quantitative data showing temporal profile of muscle atrophy in entire calf (A), tibialis anterior (TA; B), medial gastrocnemius (MG; C), lateral gastrocnemius (LG; D), soleus (SO; E) and plantaris (PL; F) muscles. Relative muscle volume, measured as percentage of their baseline values, is represented by color-coded background. * $p < 0.05$; *Student's t*-test.

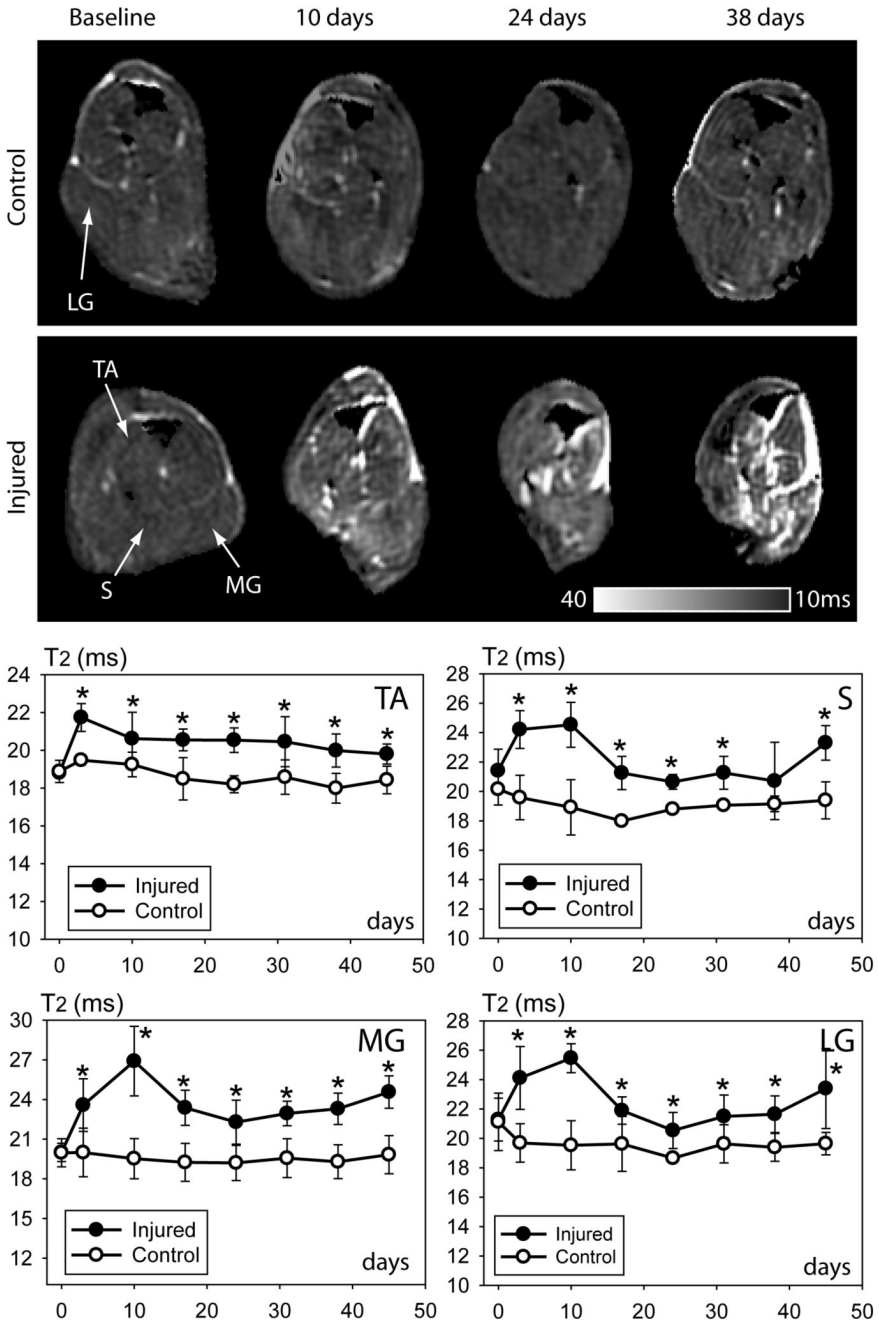

Figure 4.

Temporal changes in muscle T_2 signal after sciatic nerve axotomy. Axial T_2 maps from uninjured (top panel) and injured sides (bottom panel). MR images show progressive increase in T_2 signal in denervated muscles; increase in bright signal is also seen in tissue spaces between denervated muscles. T_2 values of denervated and uninjured muscles are shown as separate plots for four individual calf muscles. Abbreviations: LG = lateral gastrocnemius; MG = medial gastrocnemius; S = soleus; TA = tibialis anterior. * $p < 0.05$; *Student's t*-test.

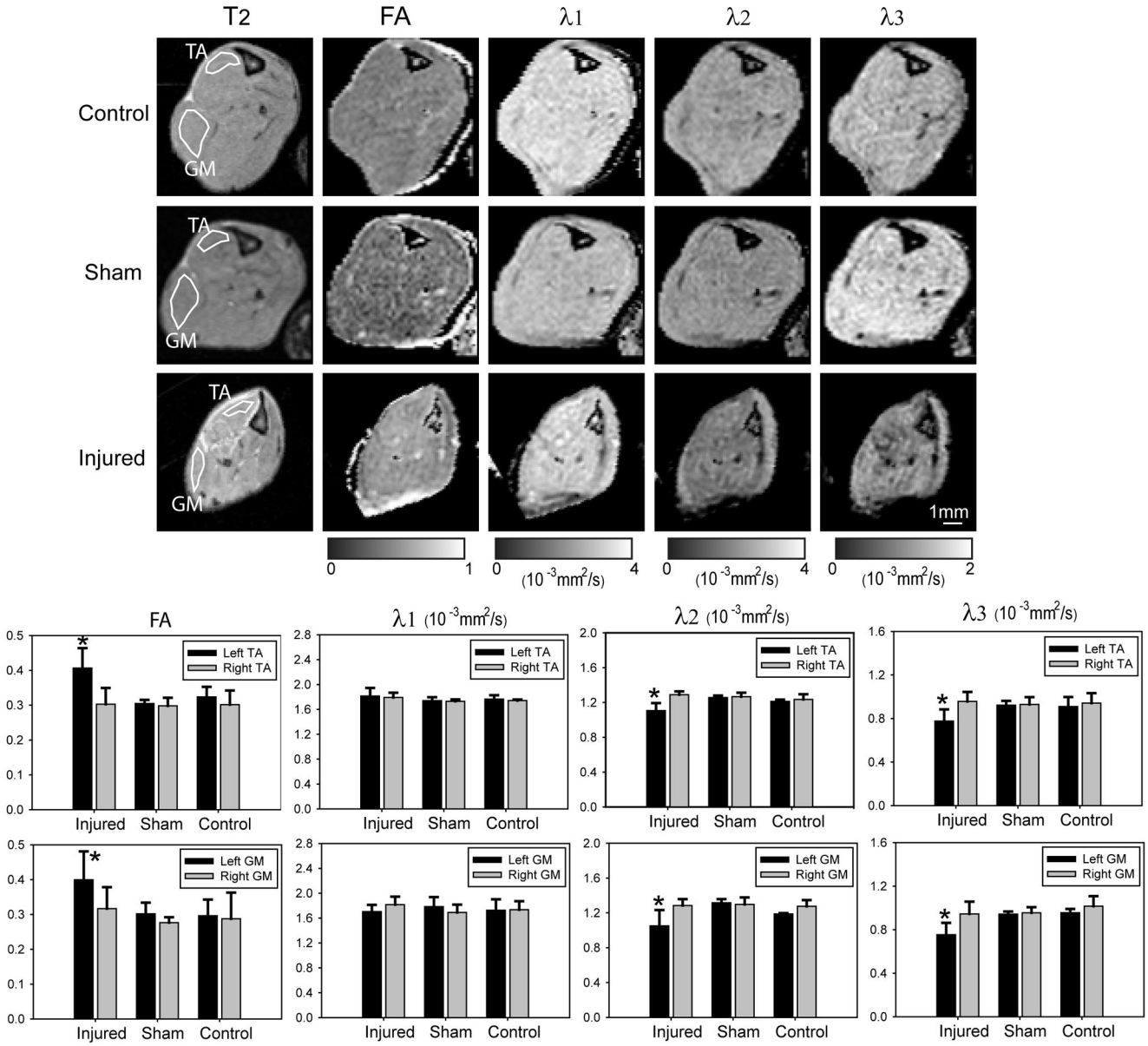

Figure 5.

Diffusion MRI of denervated muscles. Upper panel: axial images comparing T_2, fractional anisotropy (FA), and maps of three eigenvalues (λ_1, λ_2, λ_3) of calf muscles in uninjured (control), sham, and injured animals at 25 days after sciatic nerve axotomy. The data were quantified in the ROI shown in T2 images of the tibialis anterior (TA) and gastrocnemius (GM) muscles. Lower panel: Quantitative data show significant increase of FA and significant decrease of λ_2 and λ_3 in the TA and GM muscles on the injured side (left, black bars) compared to TA and GM muscles on the uninjured side (right, gray bars) and TA and GM muscles in sham and control animals. * $p < 0.05$; nonparametric rank sum test.

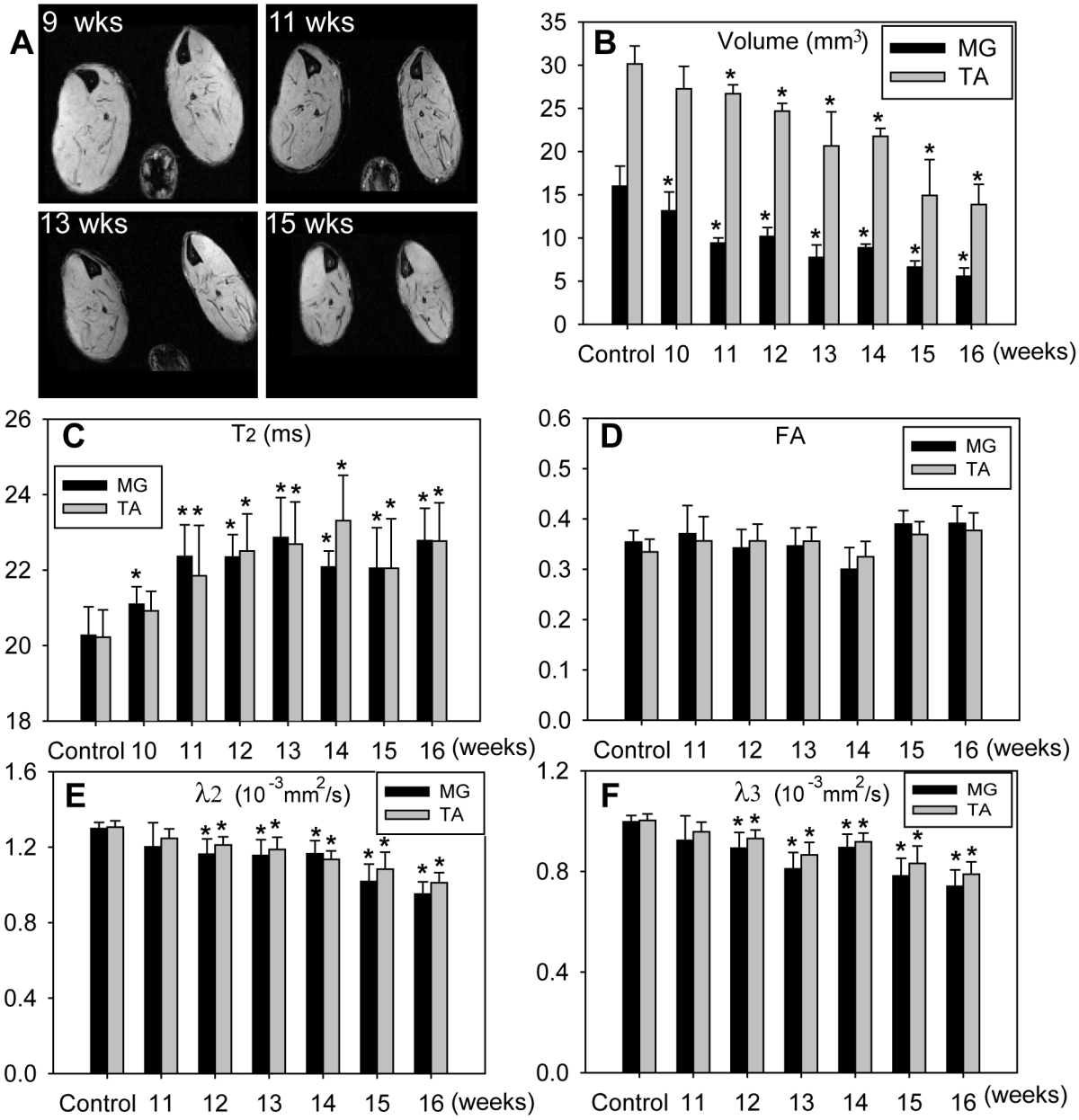

Figure 6.

Imaging data from SOD1^{G93A} mice. A: Axial images of calf muscles showing muscle volume changes at different ages. B: Changes in muscle volume in the medial gastrocnemius (MG; black bars), and the tibialis anterior (TA; gray bars) muscles at different ages. C: T_2; D: fraction anisotropy (FA); E: secondary eigenvalue (λ_2) ; F: tertiary eigenvalue (λ_3)in MG (black bars) and TA (gray bars) muscles at different ages. * $p < 0.05$; *Student's t*-test for volume measurements and T_2; nonparametric rank sum test for FA, λ_2, and λ_3.

Table 1

Temporal changes in T_2, muscle volume, secondary and tertiary eigenvalues (λ_2 and λ_3) in control and $SOD1^{G93A}$ mice.

	T_2 (ms)		Volume (mm^3) {% age of control}			$\lambda_2\{\lambda_3\}$ (10^{-3} mm^2/s)	
Age	**MG**	**TA**	**Calf**	**MG**	**TA**	**MG**	**TA**
Control	20.27 ± 0.76	20.22 ± 0.73	289.56 ± 32.55	16.00 ± 2.31	30.15 ± 2.08	1.30 ± 0.03 {1.00 ± 0.03}	1.31 ± 0.03 {1.00 ± 0.03}
10 week	21.10 ± 0.47	20.92 ± 0.52	278.29 ± 26.17 {96}	13.14 ± 2.18 {82}	27.26 ± 2.59 {90}	N/A	N/A
11 week	22.36 ± 0.84	21.85 ± 1.34	258.89 ± 67.66 {89}	9.41 ± 0.60 {59}	26.69 ± 1.04 {88}	1.20 ± 0.13 {0.92 ± 0.10}	1.25 ± 0.04 { 0.96 ± 0.04}
12 week	22.34 ± 0.60	22.51 ± 0.98	255.28 ± 42.54 {88}	10.18 ± 1.04 {64}	24.69 ± 0.89 {82 }	1.16 ± 0.08 {0.89 ± 0.06}	1.21 ± 0.04 {0.93 ± 0.03}
13 week	22.87 ± 1.06	22.69 ± 1.12	205.92 ± 59.96 {71}	7.73 ± 1.46 {48}	20.65 ± 3.95 {69}	1.15 ± 0.08 {0.81 ± 0.06}	1.19 ± 0.06 {0.87 ± 0.05}
14 week	22.08 ± 0.42	23.31 ± 1.20	216.03 ± 31.90 {75}	8.85 ± 0.44 {55}	21.76 ± 0.92 {72}	1.16 ± 0.07 {0.90 ± 0.05}	1.13 ±0.05 {0.92 ± 0.03}
15 week	22.05 ± 1.07	22.05 ± 1.31	182.34 ± 31.90 {63}	6.63 ± 0.71 {41}	14.93 ± 4.14 {50}	1.02 ± 0.09 {0.78 ± 0.07}	1.09 ± 0.09 {0.83 ± 0.07}
16 week	22.1 ± 0.78	22.12 ± 1.07	177.54 ± 35.79 {61}	6.54 ± 0.56 {41}	14.33 ± 3.12 {47}	0.95 ± 0.07 {0.74 ± 0.07}	1.01 ± 0.05 {0.79 ± 0.05}

MG = medial gastrocnemius, TA = tibialis anterior.

Table 2

Temporal changes in hind paw nerve conduction and grip strength in control and SOD1^{G93A} mice

	CMAP amplitude (mV)		Normalized Rear Leg KGF	
Ages	Control	SOD1^{G93A}	Control	SOD1^{G93A}
11 week	14.36 ± 2.46	8.98 ± 0.62	1.00 ± 0.17	0.52 ± 0.29
13 week	17.83 ± 1.80	5.79 ± 0.71	1.03 ± 0.20	0.42 ± 0.22
15 week	15.99 ± 3.21	4.31 ± 0.73	1.03 ± 0.25	0.31 ± 0.20

KGF = kilogram-force